

Journal of MARINE RESEARCH

Volume 52, Number 1

On topographic pressure drag in a zonal channel

by Alexander Krupitsky¹ and Mark A. Cane¹

ABSTRACT

The effect of bottom topography H on the barotropic transport in a periodic zonal channel is studied. An asymptotic approximation is found for the zonal transport on an f -plane and a β -plane when all f/H isolines are blocked by the zonal walls. It is shown that to leading order, the zonal channel transport is independent of friction. In this it is similar to the Sverdrup transport in a basin. To leading order, the transport is proportional to the bottom topographic wavelength, and inversely proportional to the height of the topography and to R , the range of values of f/H that exists on both sides of the channel. For sufficiently high topography the transport varies inversely with the topographic height squared. The analytic results are verified by numerical experiments.

1. Introduction

From the very beginning of Antarctic Circumpolar Current (ACC) modeling efforts it was clear that a realistic ACC transport (of the order 130 Sv [1 Sv = $10^6 \text{ m}^3/\text{s}$]; e.g. Whitworth, 1983) in a constant depth model can be obtained only with a horizontal turbulent viscosity, A_H , of the order of $10^6 \text{ m}^2/\text{s}$ (Hidaka and Tsuchiya, 1953). This is higher than the data allow. Stommel (1957, p. 178) writes: “. . . the fact that deep warm water in the Circumpolar Current preserves its Atlantic characteristics even into the Pacific Ocean suggests that the lateral diffusivity can hardly exceed $10^7 \text{ cm}^2/\text{sec}$. . .”

The ACC transport in the Bryan and Cox (1972) GFDL homogeneous global ocean model reached 650 Sv before steady state was achieved in the case of a flat bottom and $A_H = 4 \cdot 10^4 \text{ m}^2/\text{s}$; it decreased to 32 Sv when realistic topography was

1. Lamont-Doherty Earth Observatory of Columbia University, Palisades, New York, 10964, U.S.A.

introduced. Bryan and Cox (1972) explained this result by the reduction in f/H contours (f is the Coriolis parameter and H is the ocean depth) passing through the Drake Passage. Johnson and Hill (1975) have shown that any deviation from a flat bottom ocean leads to a reduction of the ACC transport. Bye and Sag (1972) concluded that “the effect of frictional processes on the circumpolar circulation is of minor importance in a variable depth model.” Ichiye (1976) attributed the underestimated ACC transport in the Bryan and Cox (1972) variable depth model to excessive horizontal viscosity. He suggested that its influence was increased by the narrowing of the jet following f/H isolines. However, according to Ichiye’s arguments the ACC transport should be inversely proportional to A_H , whereas Bryan and Cox found that ACC transport decreased only by 30% when A_H was eight times higher.

Munk and Palmen (1951) were the first to suggest that it is topographic pressure torque that balances the input of vorticity by the wind stress curl. There are significant submarine ridges which allow transfer of horizontal momentum to the solid earth. Eddy resolving numerical experiments by McWilliams *et al.* (1978), Wolff and Olbers (1989) and Wolff *et al.* (1990, 1991) have unambiguously shown topographic pressure drag to be an extremely important control on simulated ACC transport. Holloway (1987) studied the effects of topography on eddies analytically. He emphasized east-west asymmetry of the topographic drag which was shown to drive the mean flow “in the sense of intrinsic wave propagation,” i.e. westward. This result was confirmed by Wolff *et al.* (1991).

The goal of this study is to show that in the absence of horizontal viscosity, topographic pressure forces alone are able to effectively restrict barotropic transport. This is true even when the amplitude of topographic variation is relatively small. We consider a simple linear barotropic model which allows an analytical treatment. The model may be considered an extension of work by Ivanov and Kamenkovich (1959), Kamenkovich (1960, 1962) and Johnson and Hill (1975). All used essentially the same equations to study zonal channel flow in the case when there are closed f/H isolines encircling Antarctica. In this paper we focus on the case of topographic relief high enough so that all f/H isolines are blocked by the zonal walls. A study very similar to ours was simultaneously undertaken by Wang and Huang (1994). They considered a narrow ridge in an otherwise flat-bottomed channel. Their conclusions are very similar to ours in finding a quasi-Sverdrup regime in the interior of the channel. They also find similar dependencies of the transport on the parameters of the problem.

2. The model

We shall consider a barotropic current driven by a zonal wind in a periodic channel of length L_x and width L_y with bottom relief H depending only on the zonal coordinate, $H = H(x)$. L_x is also chosen as the topographic wavelength. The wind stress τ is taken to be purely zonal and depends only on latitude. We ignore all

baroclinic effects. Then, provided that the Rossby number $R_0 \ll 1$ ($R_0 = U/f_0 L_x$ where U is the horizontal velocity scale and f_0 is the mean value of the Coriolis parameter), the steady barotropic vertically integrated equations are:

$$-f\bar{v}H = gH \frac{\partial \eta}{\partial x} + \frac{\tau}{\rho_0} - r\bar{u} \quad (1)$$

$$f\bar{u}H = gH \frac{\partial \eta}{\partial y} - r\bar{v}, \quad (2)$$

$$\frac{\partial}{\partial x}(\bar{u}H) + \frac{\partial}{\partial y}(\bar{v}H) = 0, \quad (3)$$

where r is the bottom friction coefficient, η is the surface elevation and the x, y and z axes are directed eastward, southward and downward respectively. This unconventional right-handed coordinate system is convenient for the Southern hemisphere because both the depth and the Coriolis parameter are positive. Overbar represents the vertical average:

$$(\bar{u}, \bar{v}) = \frac{1}{H} \int_0^H (u, v) dz. \quad (4)$$

Horizontal viscosity terms have been omitted because we wish to show that they are unnecessary. The often used parameterization of friction in (1), (2) is the simplest and most convenient parameterization of bottom frictional processes. It is not physical; a proper parameterization would involve bottom velocity, not the barotropic velocity component. Since the bottom friction coefficient is generally believed to be small, we are primarily interested in studying the almost inviscid current. In this case the exact form of the parameterization should not be important. In view of (3) one may introduce a stream function ψ :

$$\frac{\partial \psi}{\partial x} = \bar{v}H, \quad (5)$$

$$\frac{\partial \psi}{\partial y} = -\bar{u}H. \quad (6)$$

Then dividing (1) and (2) by H and taking the curl yields

$$r \left(\frac{\partial^2 \psi}{\partial x^2} + \frac{\partial^2 \psi}{\partial y^2} - \frac{2H'}{H} \frac{\partial \psi}{\partial x} \right) + fH' \frac{\partial \psi}{\partial y} + \beta H \frac{\partial \psi}{\partial x} = -H \frac{1}{\rho_0} \frac{\partial \tau}{\partial y}. \quad (7)$$

This equation states that the wind stress curl is balanced by the bottom friction, topographic pressure torque and the β -effect (the first, second and third terms on the left-hand side, respectively).

The solution to (7) with no flow through the boundaries $y = 0, L_y$, is an L_x -periodic function:

$$\psi(x = 0) = \psi(x = L_x), \quad (8)$$

$$\psi(y = 0) = 0, \quad (9)$$

$$\psi(y = L_y) = -T. \quad (10)$$

We note that (9) and (10) are somewhat artificial for the ACC, since they imply that the current is confined between solid walls. This condition will be relaxed in a sequel to the present work.

Kamenkovich (1961) showed that the constant T , i.e. total zonal transport in the current, can be determined by integrating (1) along either side wall. Alternatively it can be found by integrating (1) along any other latitude circle (Kamenkovich, personal communication). Making use of the continuity of surface elevation η yields

$$-\int_0^{L_x} \frac{f}{H} \frac{\partial \psi}{\partial x} dx = r \int_0^{L_x} \frac{1}{H^2} \frac{\partial \psi}{\partial y} dx + \frac{1}{\rho_0} \int_0^{L_x} \frac{\tau}{H} dx, \quad 0 \leq y \leq L_y. \quad (11)$$

We will consider small depth variations: $\delta = A/H_0 \leq O(10^{-1})$, where A is the relief height scale and H_0 is the mean ocean depth. Then at the sidewalls (11) implies

$$\langle \bar{u} \rangle \approx \frac{\langle \tau \rangle}{\rho_0 r}, \quad y = 0, L_y, \quad (12)$$

where angular brackets denote the zonal average and (9), (10) are used.

It is convenient to nondimensionalize the equations. Denoting dimensional variables with asterisks, define nondimensional variables by

$$\begin{aligned} x_* &= L_x x, & y_* &= L_x y, & \tau_* &= \tau^0 \tau, \\ \beta &= \frac{L_x \beta_*}{f_0}, & f &= 1 + \beta(y - a/2), \\ H_* &= H_0 + Ah = H_0(1 + \delta h) = H_0 H, \end{aligned} \quad (13)$$

where h is $O(1)$ nondimensional topography, $\delta \lesssim O(10^{-1})$, and a is the aspect ratio

$$a = \frac{L_y}{L_x}. \quad (14)$$

Define a velocity scale

$$U = \frac{\tau^0}{f_0 \rho_0 H_0}; \quad \bar{u}_* = U \bar{u}, \quad \psi_* = \frac{U H_0 L_y}{a} \psi. \quad (15)$$

Eq. (7) becomes

$$\epsilon \left(\frac{\partial^2 \psi}{\partial x^2} + \frac{\partial^2 \psi}{\partial y^2} - \delta \frac{2h'}{H} \frac{\partial \psi}{\partial x} \right) + f \delta h' \frac{\partial \psi}{\partial y} + \beta H \frac{\partial \psi}{\partial x} = -H \frac{\partial \tau}{\partial y}, \quad (16)$$

where

$$\epsilon = \frac{r}{f_0 H_0}. \quad (17)$$

We shall explore how the principle parameters affect the total zonal transport T . If $H = \text{const}$ then (12) holds everywhere; in nondimensional form

$$\langle \bar{u} \rangle = \frac{\langle \tau \rangle}{\epsilon}. \quad (18)$$

Thus with constant H the zonal current transport is inversely proportional to the bottom friction coefficient. Since the observations of the ACC indicate that $\langle \bar{u}_* \rangle = O(0.1 \text{ m/s})$ and since $\tau = O(0.1 \text{ N/m}^2)$, the unrealistically large value $r = O(10^{-3} \text{ m/s})$ is required in a constant depth model.

We now consider the effects of variable bottom topography. It is well known that streamlines of the zonal channel current tend to follow lines of constant f/H (Ivanov and Kamenkovich, 1959). Two dynamically distinct situations arise. If the topography is small enough, then there are closed f/H isolines encircling Antarctica and a rather large transport results. There is a minimum value of the topographic height $\delta = \delta_{cr}$, where f/H lines no longer close: one f/H isoline just crosses the channel from side to side. This occurs for the value δ_{cr} such that

$$\frac{f(y=0)}{1 - \delta_{cr}} = \frac{f(y=a)}{1 + \delta_{cr}},$$

or

$$\delta_{cr} = \frac{f(y=a) - f(y=0)}{f(y=a) + f(y=0)} = \frac{a\beta}{2}. \quad (19)$$

With $\beta_* = 1.3 \cdot 10^{-11} \text{ m}^{-1}\text{s}^{-1}$, $L_y = 1000 \text{ km}$, $f_0 = 10^{-4} \text{ s}^{-1}$ $\delta_{cr} = 0.065$. If $\delta > \delta_{cr}$ there is a range R of f/H lines that intersect both walls:

$$\begin{aligned} R &= \max(f/H)_{y=0} - \min(f/H)_{y=a} \\ &= \frac{1 - a\beta/2}{1 - \delta} - \frac{1 + a\beta/2}{1 + \delta} = \frac{2}{1 - \delta^2} (\delta - \delta_{cr}) \approx 2(\delta - \delta_{cr}) \end{aligned} \quad (20)$$

Kamenkovich (1962) showed that in the small topography case $\delta < \delta_{cr}$ the transport is inversely proportional to the friction parameter ϵ as in (18). In this paper we consider the case $\delta > \delta_{cr}$ where all f/H isolines originate and terminate at zonal walls.

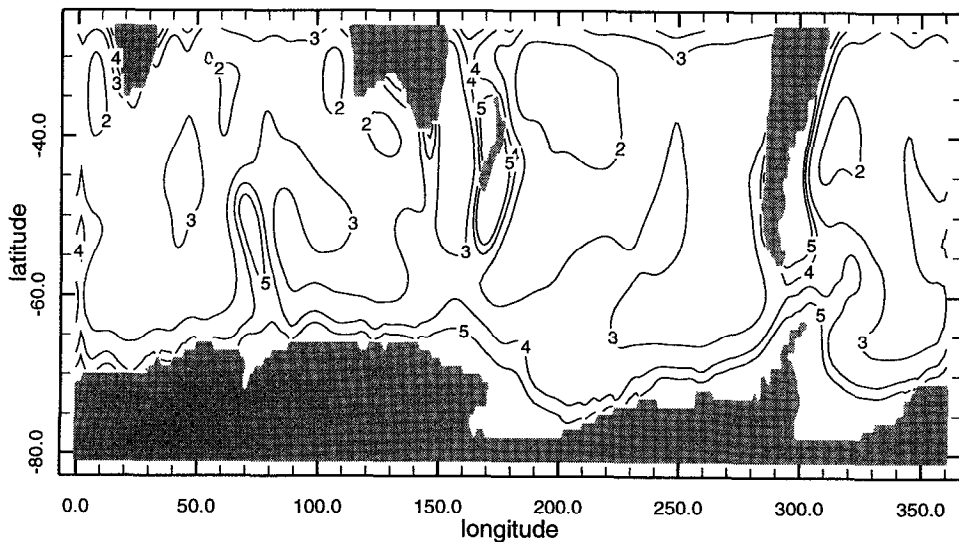


Figure 1. Map of f/H isolines, drawn using ETOPO5 (5×5 minutes Navy database) brought to one degree scale and smoothed. Units are $10^{-8} \text{ m}^{-1} \text{s}^{-1}$.

This case appears to be more applicable to the real ocean, cf. Figure 1. It will become clear from the discussion below that the dynamics of the zonal current in the two cases are quite different and that the stream function cannot be scaled to make $\psi = O(1)$ in both cases.

3. *f*-plane channel

We begin with the case of the *f*-plane ($\beta = 0$) channel. Since $H = H(x)$ all f/H contours are meridional. Consider (16) with $f = 1$ and $\beta = 0$

$$\epsilon \left(\frac{\partial^2 \psi}{\partial x^2} + \frac{\partial^2 \psi}{\partial y^2} - \delta \frac{2h' \partial \psi}{H \partial x} \right) + \delta h' \frac{\partial \psi}{\partial y} = -H \frac{\partial \tau}{\partial y}. \quad (21)$$

In the vicinity of lines $h' = 0$ ($-\lambda < h' < \lambda$; $\lambda \ll 1$) internal boundary layers arise. Away from these boundary layers we find an interior solution by neglecting the friction terms and integrating (21) along the characteristics $H = \text{const}$ starting from the southern wall when $h' > 0$ and from the northern wall when $h' < 0$:

$$\psi = \begin{cases} -T - \frac{H}{\delta h'} (\tau - \tau_a) & h' \gg \lambda, y > \Delta \\ -\frac{H}{\delta h'} (\tau - \tau_0) & h' \ll -\lambda, y < a - \Delta \end{cases} \quad (22)$$

where $\tau_a = \tau(a)$ and $\tau_0 = \tau(0)$.

At the far wall (northern for $h' > 0$; southern when $h' < 0$) there is a boundary layer similar to that studied by Stommel (1948). It is required to satisfy the sidewall boundary condition (9) or (10). Within these layers the boundary layer stream function may be found from the approximation to (21):

$$\epsilon \frac{\partial^2 \Psi}{\partial y^2} + \delta h' \frac{\partial \Psi}{\partial y} = 0;$$

the thickness of these layers is $\Delta = O(\epsilon/\delta)$. Note that the boundary layer changes its position from one wall to the other when the sign of the bottom slope changes; the two sides are connected by internal, cross-channel layers centered on $h' = 0$ lines.

With the exception of these boundary layers, the circulation consists of alternating closed gyres trapped between lines where h' changes sign. Thus all net transport is concentrated in the boundary current which crosses the channel from side to side in the internal boundary layers where $h' = 0$. The stream function undergoes sharp changes across topographic extrema, with the internal part of the boundary layer at $h' = 0$ lines connecting the pieces of the boundary layer along the zonal walls (Fig. 2). A similar example of an internal boundary layer may be found in Kamenkovich and Mitrofanov (1971).

As shown in the Appendix, applying the nondimensional version of condition (11) to (22) yields

$$T = O(\delta^{-1}) \quad (23)$$

for a general wind stress. If $\tau(0) = \tau(a) = 0$ the leading order terms vanish and the residual terms yield $T \rightarrow 0$ as $\epsilon \rightarrow 0$ (see Appendix).

Streamline plots calculated numerically for selected parameter values are shown in Figure 2. The topography used here is

$$h = \begin{cases} 4x, & 0 \leq x \leq \frac{1}{4} \\ 2 - 4x, & \frac{1}{4} \leq x \leq \frac{3}{4} \\ 4x - 4, & \frac{3}{4} \leq x \leq 1. \end{cases} \quad (24)$$

Of course, (24) is not the real topography. It is a simple example to demonstrate that even relatively small topography [$\delta = O(0.1)$] exerts a very strong effect on the zonal current. We used a new barotropic solver developed at L-DEO (Naik *et al.*, 1994). The method employs a compact fourth order discretization, based on analytic solutions of one-dimensional problems. It has advantages over conventional solvers for cases with narrow boundary layers.

In all cases the circulation consists of two alternating closed symmetric gyres and a boundary layer jet moving between north and south walls where $h' = 0$. The following parameters were used in all experiments: $f_0 = 10^{-4} \text{ s}^{-1}$, $H_0 = 4 \text{ km}$, $L_y =$

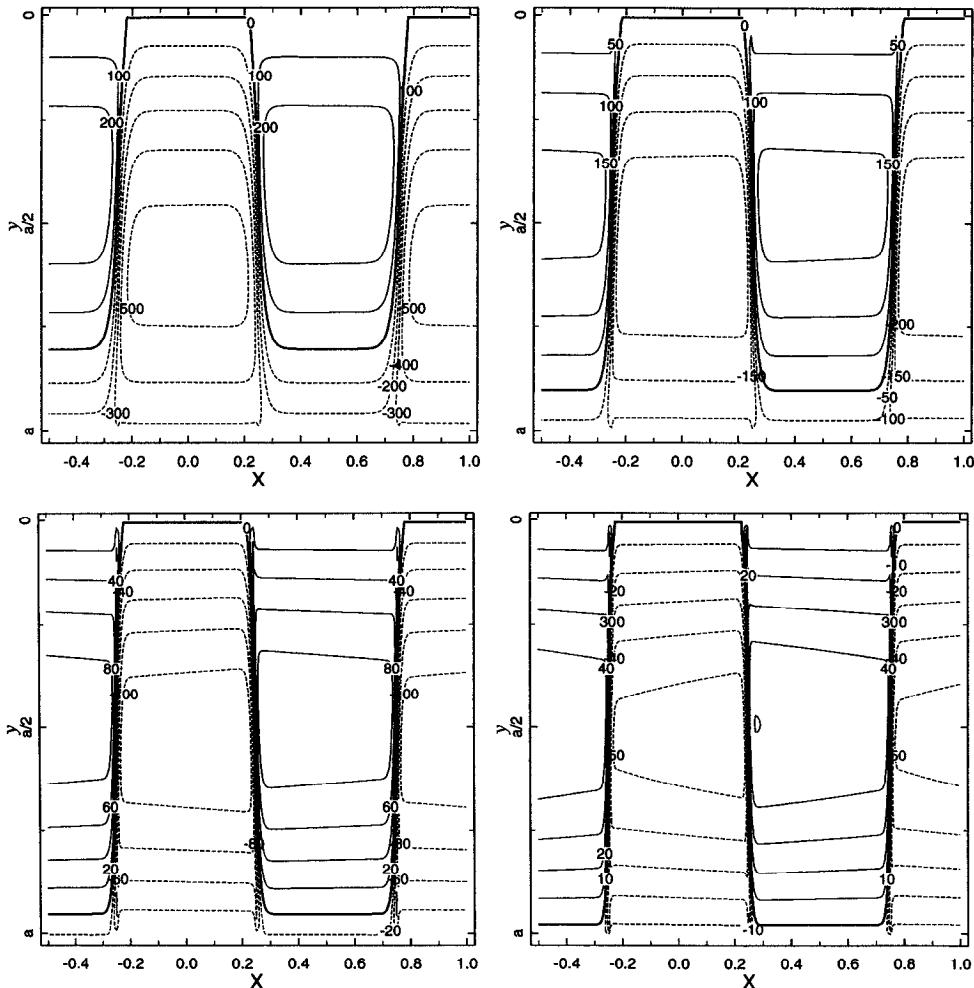


Figure 2. Stream function isolines (Sv) in an f -plane channel calculated numerically using (21), (8)–(10). The additional half-period $[-0.5, 0]$ was added to improve the view of the two gyre system. Topography is given by (24); wind stress is specified by (25); $\epsilon = 2.5 \cdot 10^{-4}$, $a = 0.1$. (a) $\delta = 6.25 \cdot 10^{-3}$, (b) $\delta = 1.25 \cdot 10^{-2}$, (c) $\delta = 2.5 \cdot 10^{-2}$, (d) $\delta = 5 \cdot 10^{-2}$.

1000 km , $\tau^0 = 0.1 \text{ N/m}^2$, $\rho_0 = 10^3 \text{ kg/m}^3$ and

$$\tau = \sin\left(\frac{\pi y}{a}\right). \quad (25)$$

The value $r = 10^{-4} \text{ m/s}$ used in most of the experiments is one order of magnitude less than needed to yield a realistic transport value in the constant depth model: (18) implies a value of 2500 Sv. The dependencies of the transport on ϵ , δ calculated

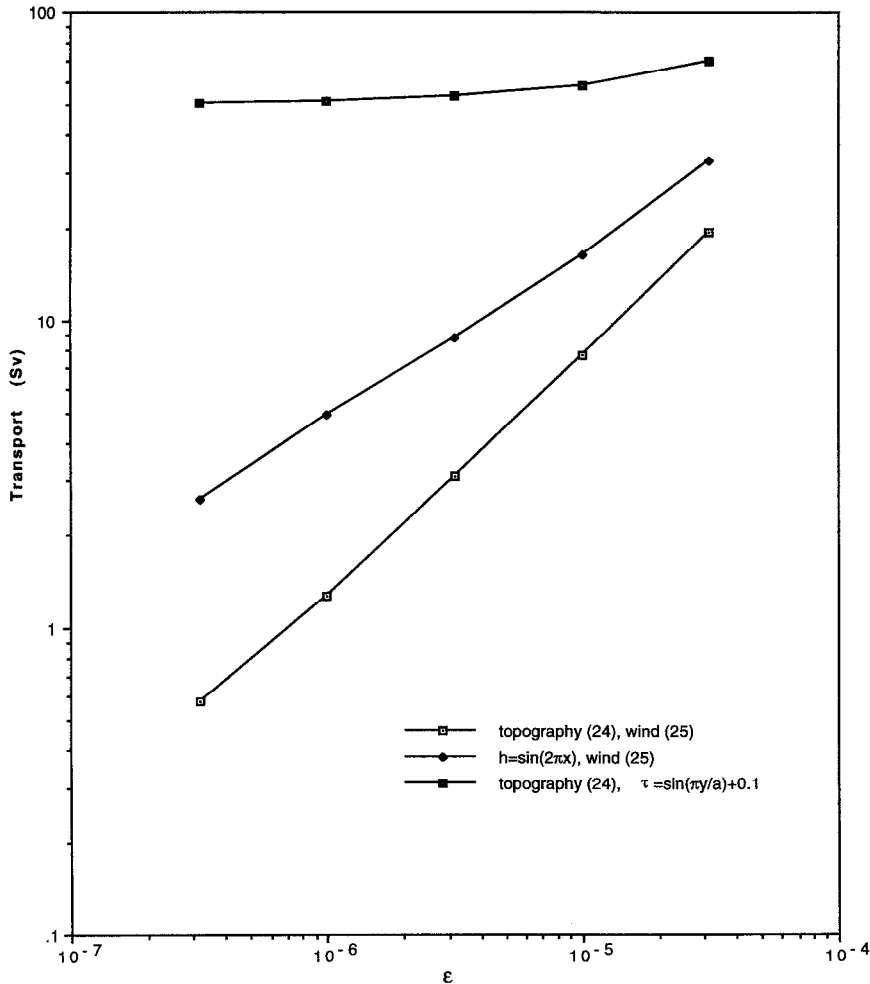


Figure 3. f -plane channel transport calculated numerically; $a = 0.1$. (a) as a function of ϵ , $\delta = 0.1$; (b) as a function of δ , $\epsilon = 10^{-6}$

numerically using (21), (25) for topography (24) and $h = \sin(2\pi x)$ are shown in Figure 3a, b.

4. β -plane channel

Introduce new orthogonal coordinates (ξ, η) , along and across the gradient of f/H :

$$\nabla \eta = \frac{1}{\delta} \nabla \left(\frac{f}{H} \right) = \frac{1}{\delta} \left(-\frac{f H'}{H^2}, \frac{\beta}{H} \right), \quad (26a)$$

$$\nabla \xi = -(\beta H/H', f). \quad (26b)$$

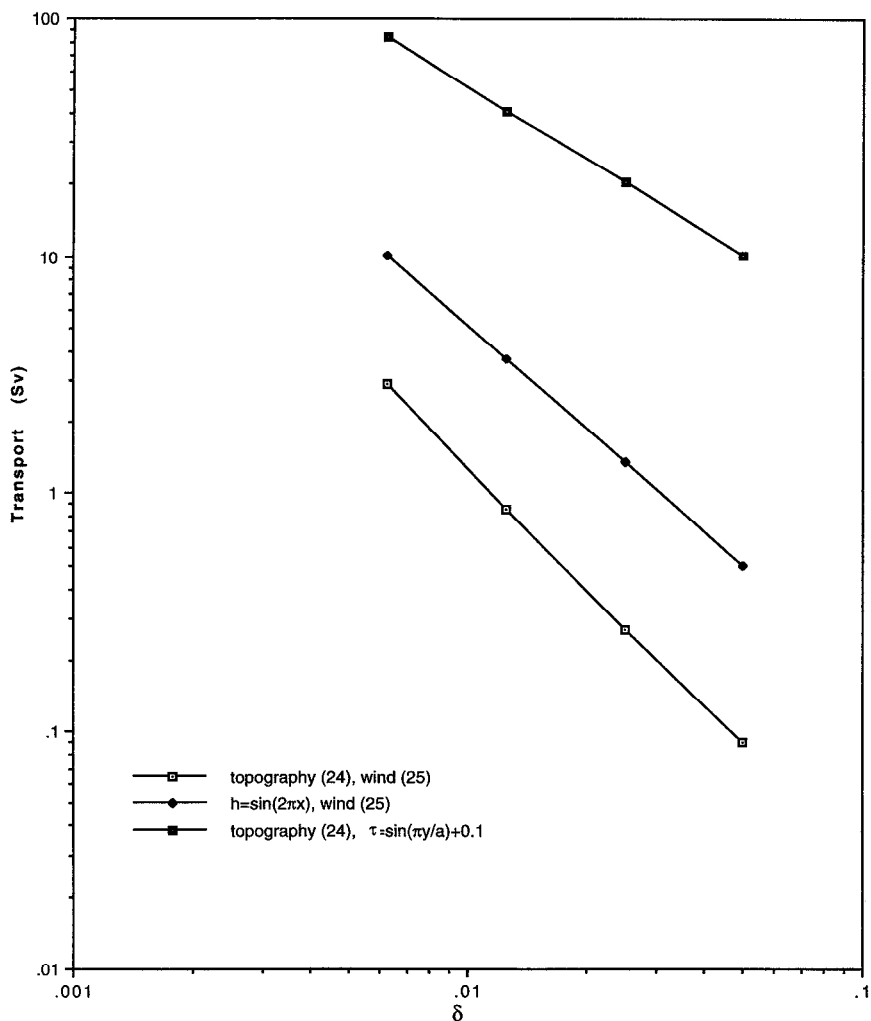


Figure 3. (Continued)

In these coordinates (16) reads

$$\epsilon \bar{\Delta} \psi + \delta H^2 J(\xi, \eta) \frac{\partial \psi}{\partial \xi} = -H \frac{\partial \tau}{\partial y} \quad (27)$$

where

$$\bar{\Delta} = |\nabla \eta|^2 \frac{\partial^2}{\partial \eta^2} + |\nabla \xi|^2 \frac{\partial^2}{\partial \xi^2} + (\Delta \eta) \frac{\partial}{\partial \eta} + (\Delta \xi) \frac{\partial}{\partial \xi}, \quad (28)$$

$$\Delta = \frac{\partial^2}{\partial x^2} + \frac{\partial^2}{\partial y^2}, \quad (29)$$

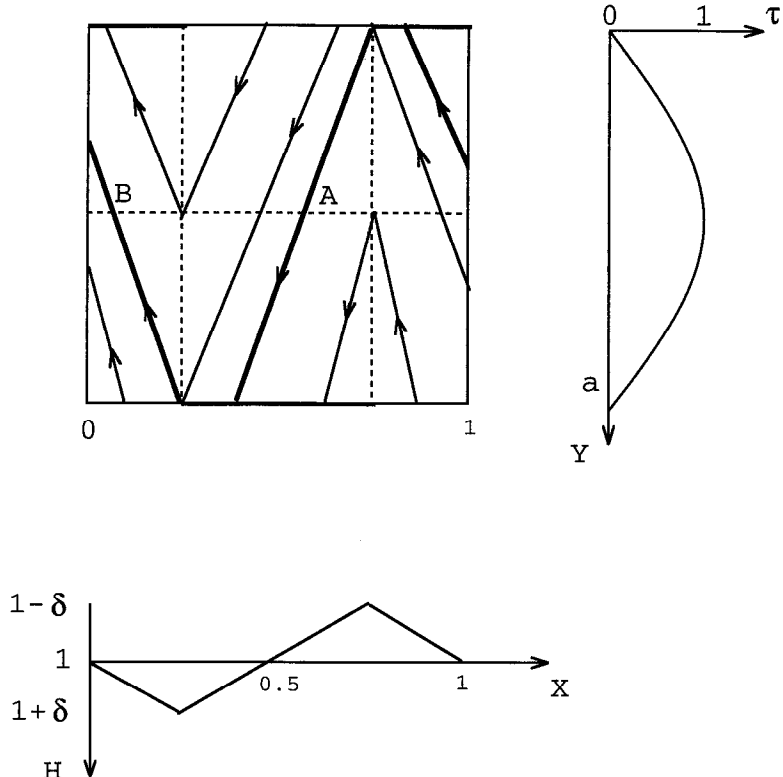


Figure 4. A schematic of the characteristics f/H , wind stress and model topography. Points A and B are discussed in the text.

$$J(\xi, \eta) = \frac{\partial \xi}{\partial x} \frac{\partial \eta}{\partial y} - \frac{\partial \xi}{\partial y} \frac{\partial \eta}{\partial x} = - \frac{\beta^2 H^2 + f^2 \delta^2 h'^2}{\delta^2 H^2 h'} \quad (30)$$

and the small term of order $\epsilon \delta$ has been omitted.

Since the friction parameter ϵ is very small, the zero order solution is readily found by integration of the inviscid version of (27)

$$\delta H^2 J(\xi, \eta) \frac{\partial \psi}{\partial \xi} = -H \frac{\partial \tau}{\partial y} \quad (31)$$

along the characteristics, i.e., lines of constant η :

$$\psi(\xi) - \psi(\xi_0) = - \int_{\xi_0}^{\xi} \frac{1}{\delta J(\xi, \eta) H} \frac{\partial \tau}{\partial y} \Big|_{\eta} d\xi \quad (32a)$$

or

$$\psi(x, \eta) - \psi(x_0, \eta) = - \int_{x_0(\xi_0)}^{x(\xi)} \frac{1}{\delta J(\xi, \eta) H} \left(\frac{\partial \tau}{\partial y} \frac{\partial \xi}{\partial x} \right) \Big|_{\eta} dx' \quad (32b)$$

where (x_0, y_0) is the origin of the characteristic which connects the point $x(\xi, \eta)$ with the sidewall (the direction of integration is shown in Fig. 4).

Since

$$\begin{aligned} \left. \frac{\partial \xi}{\partial x} \right|_{\eta} &= \left. \frac{\partial \xi}{\partial x} \right|_y + \left. \frac{\partial \xi}{\partial y} \right|_x \left. \frac{\partial y}{\partial x} \right|_{\eta} = \frac{J(\xi, \eta)}{\partial \eta / \partial y}, \\ \psi(x, \eta) &= \psi(x_0, \eta) - \int_{x_0}^x \frac{1}{\beta} \left. \frac{\partial \tau}{\partial y} \right|_{\eta} dx'. \end{aligned} \quad (32c)$$

As long as $dy/dx' = \eta^{-1}\beta/H' \neq 0$ along the characteristic, (32c) may be rewritten as

$$\psi(x, y) = \psi(x_0, y_0) - \eta^{-1} \int_{y_0}^y \left. \frac{\partial \tau / \partial y}{H'} \right|_{\eta} dy'. \quad (32d)$$

A schematic of the characteristics of (31), $\eta \equiv f/H = \text{constant}$, is given in Figure 4. The direction of integration, shown in Figure 4 by arrows, is determined from (31). As in the Stommel problem or the f -plane problem of the last section, consideration of which side allows a boundary layer dictates integrating in the direction of $\nabla \xi$ when $H' > 0$ and $-\nabla \xi$ when $H' < 0$. The location of boundary layers is shown by bold lines. Boundary layers arise at the sidewalls, where characteristics end, and inside the channel, where critical characteristics separate regions in which information comes from the opposite walls. We consider only the case $\delta > \delta_c$, where no f/H isolines close in the channel. Then there are a number of cross-channel f/H isolines with the critical characteristic η_c being the westernmost. In the vicinity of the critical characteristics we write

$$\psi = \psi_I + \tilde{\psi}, \quad (33)$$

where ψ_I is the interior solution satisfying (32) and $\tilde{\psi}$ is the boundary layer correction term near $\eta = \eta_c$. Substituting (33) into (27) one finds the equation for $\tilde{\psi}$

$$\epsilon \bar{\Delta} \tilde{\psi} + H^2 J(\xi, \eta) \frac{\partial \tilde{\psi}}{\partial \xi} = -\epsilon \bar{\Delta} \psi_I. \quad (34)$$

Since the gradients are larger across the boundary layer than along it, it is the term proportional to $\partial^2 \tilde{\psi} / \partial \eta^2$ which balances the second term of (34) in the internal boundary layer. To leading order, after substituting (26) into (34):

$$\epsilon \frac{\beta^2 H^2 + f^2 \delta^2 h'^2}{\delta^2 H^4} \left[\frac{\partial^2 \tilde{\psi}}{\partial \eta^2} + \frac{\partial^2 \psi_I}{\partial \eta^2} \right] - \frac{\beta^2 H^2 + f^2 \delta^2 h'^2}{\delta h'} \frac{\partial \tilde{\psi}}{\partial \xi} = 0,$$

or simply (as long as $\beta \neq 0$)

$$\frac{\epsilon}{\delta} h' \frac{\partial^2 \tilde{\psi}}{\partial \eta^2} - H^4 \frac{\partial \tilde{\psi}}{\partial \xi} = -\frac{\epsilon h'}{\delta} \frac{\partial^2 \psi_I}{\partial \eta^2}. \quad (35)$$

We will not need to solve (35). It will be sufficient to note that the internal boundary layer width is $O((\epsilon/\delta)^{1/2})$. It is interesting that, as in the f -plane case, the near-wall

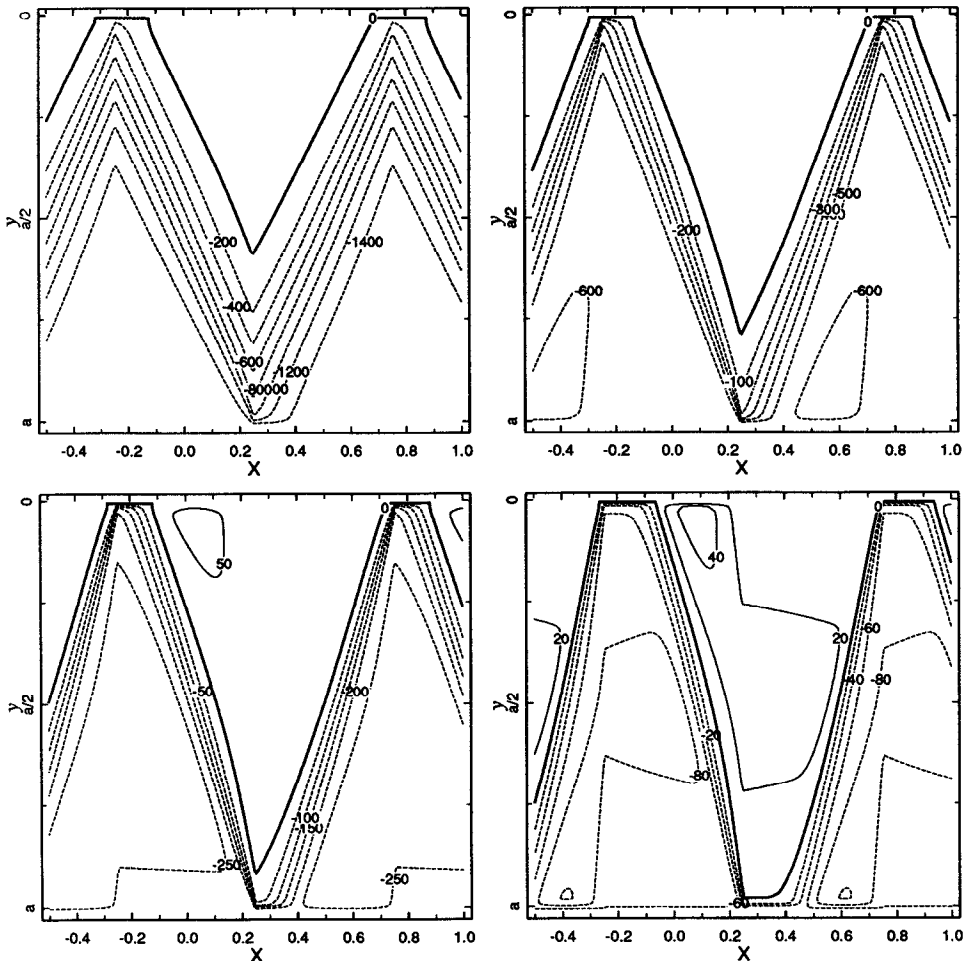


Figure 5. Stream function isolines (Sv) in a β -plane channel calculated numerically from (16), (24) with the wind stress (25); $\beta = 0.13a^{-1}$. (a) $\delta = 5 \cdot 10^{-2}$; (b) $\delta = \delta_{cr} = 6.5 \cdot 10^{-2}$; (c) $\delta = 7.5 \cdot 10^{-2}$; (d) $\delta = 0.1$. Other parameters and forcing are the same as in Figure 2. Since $\delta_{cr} = 6.5 \cdot 10^{-2}$ ($A_{cr} = 260$ m) all f/H isolines are blocked in (c), (d).

boundary layer width is $O(\epsilon/\delta)$: the internal boundary layer is substantially wider. One can observe this feature in Figure 5c, d. It is convenient to set $\epsilon = O(\delta^3)$ to express all the parameters in terms of δ , the parameter of primary interest. Then the internal boundary layer width $\lambda = O(\delta)$.

We shall find the transport using the nondimensional auxiliary condition (11) applied at $y = a/2$:

$$-\int_0^1 \frac{1}{H} \frac{\partial \psi}{\partial x} dx = \int_0^1 \frac{\tau}{H} dx + \epsilon \int_0^1 \frac{1}{H^2} \frac{\partial \psi}{\partial y} dx. \quad (36)$$

After integration by parts, the left-hand side of (36) can be written using (32c) as

$$-\int_0^1 \frac{1}{H} \frac{\partial \psi}{\partial x} dx = \int_0^1 \psi(x_0, y_0) \frac{dH^{-1}}{dx} dx - \left[\frac{\int_{-1/4}^B}{I_1} + \frac{\int_B^{1/4}}{I_2} + \frac{\int_{1/4}^A}{I_3} + \frac{\int_A^{3/4}}{I_4} \right] \frac{dH^{-1}}{dx} \int_{x_0}^x \frac{1}{\beta} \frac{\partial \tau}{\partial y} \Big|_{\eta} dx' dx, \quad (37)$$

where A, B are the intersections of the critical characteristics with the line center $y = a/2$ (Fig. 4). The points A, B are defined by

$$\frac{f(a/2)}{H(A)} = \frac{f(0)}{H_{\min}}, \quad \frac{f(a/2)}{H(B)} = \frac{f(a)}{H_{\max}}$$

so

$$H(A) = \frac{1 - \delta}{1 - \delta_{cr}}, \quad H(B) = \frac{1 + \delta}{1 + \delta_{cr}}. \quad (38)$$

Since $\psi(x_0, y_0) = 0$ for $B < x < A$ and $\psi(x_0, y_0) = -T$ otherwise,

$$\int_0^1 \psi(x_0, y_0) \frac{dH^{-1}}{dx} dx = -TH^{-1} \Big|_{-1+A}^B = \frac{2(\delta - \delta_{cr})}{1 - \delta^2} T = 2(\delta - \delta_{cr})T + O(\delta^2 T). \quad (39)$$

It is straightforward to show that the contribution of the interior boundary layer corrections ψ of (35) is $O(\delta^2 T)$. For the integrals I_2, I_4 it is convenient to split the internal integrals at the extrema of H where dy/dx changes sign (Fig. 4). For example for I_2

$$\int_{x_0}^x \frac{1}{\beta} \frac{\partial \tau}{\partial y} \Big|_{\eta} dx' = \int_{x_0}^{1/4} \frac{1}{\beta} \frac{\partial \tau}{\partial y} \Big|_{\eta} dx' + \int_{1/4}^x \frac{1}{\beta} \frac{\partial \tau}{\partial y} \Big|_{\eta} dx', \quad (40)$$

The integrals I_1, I_3 and the first terms on the right of (40) in the integrals I_2, I_4 can be evaluated as in (32d):

$$\int_{x_0}^x \frac{1}{\beta} \frac{\partial \tau}{\partial y} \Big|_{\eta} dx' = \eta^{-1} \int_{y_0}^y \frac{\partial \tau / \partial y}{H'} dy = \eta^{-1} \{(H')^{-1}\} [\tau(y) - \tau(y_0)], \quad (41)$$

where the braces denote the appropriate average. This average exists if the topography is reasonably well behaved. We further assume that

$$\{(H')^{-1}\} = \frac{1}{H'(x_1)} (1 + O(\delta)) \approx \frac{1}{H'(x_1)}, \quad (42)$$

where x_1 is the point where the characteristic $\eta = \eta(x)$ crosses $y = a/2$ (i.e. x_1 is the point such that $H(x_1) = H(x)$; for I_1, I_3 and the second terms on the right of (40) $x_1 = x$). Eq. (42) will hold if either: (i) there is little change in x between y_0 and $a/2$

(e.g. $\delta \gg \delta_{cr}$) or (ii) there is little curvature. For the piecewise linear profile (24) the curvature is zero and this is exact. Numerical experiments show that this approximation has a negligible effect on the final result in all cases considered here due to the assumed symmetry of the topography and forcing.

Since we assume $\tau = 0$ at the sidewalls, and since $\eta^{-1}(x, a/2) = H(x)$, using (41) and (42) in (38) and (40) results in

$$\begin{aligned} -\int_0^1 \frac{1}{H} \frac{\partial \Psi}{\partial x} dx &\approx 2(\delta - \delta_{cr})T + \int_0^1 \frac{\tau}{H} dx \\ &+ \int_B^{1/4} \frac{dH(x)^{-1}}{dx} H(x) \tau(y_*(1/4, x)) \left[\frac{1}{H'(x)} - \frac{1}{H'(x_1)} \right] dx \\ &+ \int_A^{3/4} \frac{dH(x)^{-1}}{dx} H(x) \tau(y_*(3/4, x)) \left[\frac{1}{H'(x)} - \frac{1}{H'(x_1)} \right] dx, \end{aligned} \quad (43)$$

where the y_* 's, the intersections of the characteristics with the lines $x = 1/4$ and $x = 3/4$, respectively, are determined by

$$\frac{1}{H(x)} = \frac{1 + \beta(y_* - a/2)}{1 \pm \delta} \quad (44)$$

(The plus sign applies for $x = 1/4$, the minus sign for $x = 3/4$.) Assuming symmetry about the extrema of H implies $H'(x_1) = -H'(x)$. Now substituting (43) in (36) yields

$$2(\delta - \delta_{cr})T = 2 \int_B^{1/4} \frac{\tau(y_*)}{H} dx + 2 \int_A^{3/4} \frac{\tau(y_*)}{H} dx.$$

Since the range of y_* is $(a/2, a)$ in the first integral and $(0, a/2)$ in the second, the transport is a weighted integral of the wind stress at all latitudes. With an approximation similar to (42) and changing the variable of integration according to (44) we obtain

$$(\delta - \delta_{cr})T = -\frac{\beta}{H'(B)} \int_a^{a/2} \tau(y) dy - \frac{\beta}{H'(A)} \int_0^{a/2} \tau(y) dy. \quad (45)$$

With the wind (25)

$$(\delta - \delta_{cr})T = \frac{\beta a}{\pi} \left[\frac{1}{H'(B)} - \frac{1}{H'(A)} \right] \quad (46)$$

With the piecewise linear topography (24) $H'(B) = -H'(A) = 4\delta$, hence

$$T = \frac{\delta_{cr}}{\pi \delta (\delta - \delta_{cr})} \quad (47)$$

to leading order.

This is an asymptotic approximation to the transport in the case $\delta > \delta_{cr}$. The transport is inversely proportional to the topographic height δ and to the range of values of cross-channel f/H isolines $R = 2(\delta - \delta_{cr})$; hence for $\delta \gg \delta_{cr}$ it varies inversely as δ^2 and does not depend on friction to leading order.

In dimensional units (47) reads

$$T_* = \frac{\beta_* L_y L_x H_0^2 \tau^0}{\pi A f_0 \rho_0 (2A f_0 - \beta_* H_0 L_y)} \quad (47')$$

The validity of (47) is based on the assumption $\epsilon \leq O(\delta^3)$. For larger values of ϵ the solution to (16) will be jointly controlled by topographic pressure drag and friction. The critical value $\delta = \delta_{cr}$ marks the transition from the frictionally controlled flow regime to the topographically controlled one.

Since the transport is independent of dissipation to leading order it is interesting to study the energy budget in the limit of very small friction. It follows from (31) that $\partial\psi/\partial\eta$ is negligible compared to $\partial\psi/\partial\xi$. Hence to leading order

$$\frac{\partial\psi}{\partial y} = \frac{\partial\psi\partial\xi}{\partial\xi\partial y} = - \frac{f\delta h' H}{\beta^2 H^2 + f^2 \delta^2 h'^2} \frac{\partial\tau}{\partial y}, \quad (48)$$

where use is made of (26b) and (31). The zero order total energy input is

$$-\int_0^1 dx \int_0^a \frac{\tau}{H} \frac{\partial\psi}{\partial y} dy = \left(\delta \int_0^a f\tau \frac{\partial\tau}{\partial y} dy \right) \left(\int_0^1 \frac{h'}{\beta^2 H^2 + f^2 \delta^2 h'^2} dx \right). \quad (49)$$

It follows from (49) that the net total energy input vanishes to leading order, if we assume that $H(x)$ is symmetric with respect to lines where $dH/dx = 0$. In the more general case where the total energy input is non-zero to leading order the dissipation needed to balance it occurs in the boundary layers (see Discussion).

Now we proceed to verify the analytic results with numerical solutions to (16) with the topography (24) and wind (25).

The solution is sought as

$$\psi = \psi_1 + T\psi_2,$$

where ψ_1 satisfies (16) and the boundary conditions

$$\psi_1(y = 0) = \psi_1(y = a) = 0,$$

while ψ_2 satisfies the homogeneous version of (16) and the boundary conditions

$$\psi_2(y = 0) = 0, \quad \psi_2(y = a) = -1$$

so that T may be found using the nondimensional form of (11) at $y = a/2$ (or any

other line of constant latitude):

$$T = - \frac{\int_0^1 \left(\frac{1}{H} \frac{\partial \Psi_1}{\partial x} + \frac{\epsilon}{H^2} \frac{\partial \Psi_1}{\partial y} + \frac{\tau}{H} \right) dx}{\int_0^1 \left(\frac{1}{H} \frac{\partial \Psi_2}{\partial x} + \frac{\epsilon}{H^2} \frac{\partial \Psi_2}{\partial y} \right) dx}. \quad (50)$$

When $\delta > \delta_{cr}$ circulation patterns are quite similar to those of the *f*-plane solution (Fig. 5c, 5d). Streamlines tend to follow *f/H* isolines in the major part of the domain. The broad, strong current in the case $\delta < \delta_{cr}$ (Fig. 5a, 5b) becomes very narrow and confined to the boundary layers when $\delta > \delta_{cr}$ (Fig. 5c, 5d).

Dependence of the transport on the zonal scale L_x is similar to the *f*-plane case when $\delta > \delta_{cr}$, whereas when $\delta \ll \delta_{cr}$, the β -plane channel transport is insensitive to the topographic wavelength (Kamenkovich, 1962). Qualitatively, the dependence of the transport on the relief height may be described as follows. For small δ ($\delta < \delta_{cr}$) the transport is proportional to the range of closed *f/H* isolines $R \approx 2(\delta - \delta_{cr})$ and inversely proportional to the friction parameter ϵ . For $\delta \geq 1.2\delta_{cr}$ (47') agrees well with the results of the numerical experiments (Fig. 6): the transport varies inversely as $\delta(\delta - \delta_{cr})$.

For a constant wind $\tau \equiv \tau^c$, the wind stress curl is zero so $\Psi_1 \equiv 0$. The denominator of (50) is calculated similarly to (39) and equals $2(\delta - \delta_{cr})$ to leading order. Thus

$$T_c \approx \frac{\tau^c}{2(\delta - \delta_{cr})}. \quad (51)$$

Repeating the steps (43)–(47) for the case of an asymmetric wind ($\tau(a/2 + y) = -\tau(a/2 - y)$) yields no leading order contribution

$$T_a \leq O(1). \quad (52)$$

Since the problem is linear and since any function can be represented as a sum of a symmetric and an asymmetric component, (47) can be combined with (51), (52) to yield a solution for a general wind forcing.

5. Discussion

We have investigated only one of many phenomena possibly relevant to ACC dynamics. Using a simple physical model it was shown that the zonal channel current is strongly affected by topographic pressure drag. As is well known, if closed *f/H* isolines exist, the transport is nearly independent of the topographic wavelength, proportional to the range of closed *f/H* isolines and inversely proportional to the friction parameter ϵ . Here we found an asymptotic approximation to the transport of the β -plane channel current in the case when all lines of constant *f/H* are blocked by the zonal walls. In this case the zonal transport is proportional, to a first approxima-

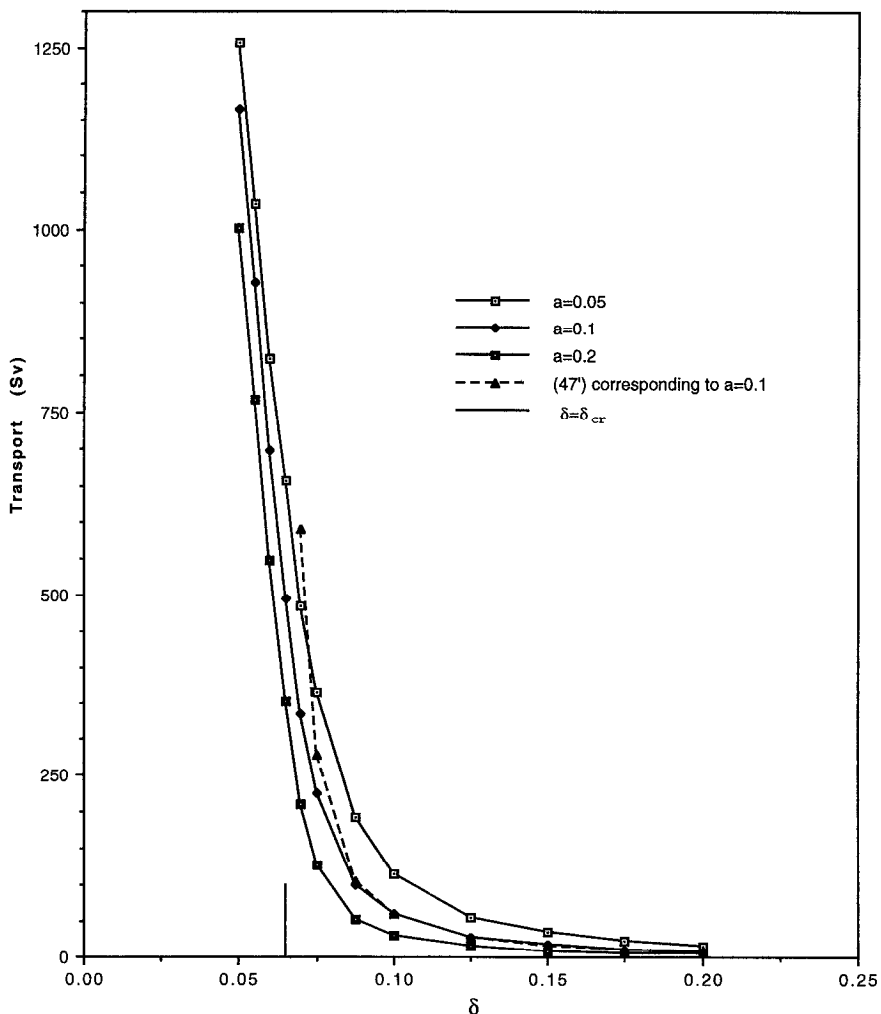


Figure 6. β -plane channel transport calculated numerically for different aspect ratios compared to (47'). Other parameters and forcing are the same as in Figure 5.

tion, to the bottom topographic wavelength, and inversely proportional to the range of values of f/H that exists on both sides of the channel, $R = 2(\delta - \delta_{cr}) = 24/H - |f_N - f_S|/f_0$ and to the topographic height δ ; when $\delta \gg \delta_{cr}$ the transport varies as δ^{-2} . The transport is independent of friction. In the case of closed f/H isolines ($\delta < \delta_{cr}$), friction is essential to dissipate the wind's input of momentum and energy, leading to an ϵ^{-1} dependence on the transport. In the blocked case ($\delta > \delta_{cr}$) studied here, the momentum input is balanced by topographic pressure drag. The energy input is

dissipated (to leading order) entirely in boundary layers. Since $L_B = O(\epsilon/\delta)$,

$$\text{Diss} = O\left(\int_0^{L_B} \epsilon \left(\frac{\partial \psi}{\partial y}\right)^2 dy\right) = O\left(\epsilon \frac{T}{L_B^2} L_B\right) = O\left(\frac{\epsilon}{L_B} T\right) = O(\delta T).$$

As in the Sverdrup-Stommel problem (Stommel, 1948) the boundary layer width L_B changes with friction to make the energy dissipation independent of friction. We saw in Section 4 that with our specific choice of symmetric bottom relief the net total energy input from the wind vanishes to leading order outside the boundary layers. The general result that to leading order the transport does not depend on friction is independent of this assumption.

The strong effect of the depth variation amplitude on the transport of the β -plane channel current is consistent with results of the eddy resolving numerical experiments of Wolff *et al.* (1990, 1991) and Treguier and McWilliams (1990) and lends support to the importance of the form drag studied here. In our simple model vertical viscosity is parameterized (artificially) to transfer momentum down the water column. It replaces the eddies which are responsible for this momentum transfer in eddy resolving models. However, in the other studies topography has a strong effect on eddies which would seem to be relevant to the real ocean. This level of complexity is completely missing in our model, which is deliberately kept simple to illuminate the effect of the bottom topography on the large-scale zonal current.

Acknowledgments. The authors are grateful to Vladimir Kamenkovich for helpful discussions and to Naomi Naik for the help in numerical aspects of the problem. AK was supported by the generous gift of the G. Unger Vetlesen Foundation. MC was supported by NSF grant OCE-9-00127.

APPENDIX

An asymptotic solution on an f -plane

It will be assumed here that $H(x)$ is symmetric with respect to lines where $dH/dx = 0$. The transport can be found by applying the nondimensional condition (11)

$$-\int_0^1 \frac{1}{H} \frac{\partial \psi}{\partial x} dx = \int_0^1 \frac{\tau_c}{H} dx + \epsilon \int_0^1 \frac{1}{H^2} \frac{\partial \psi}{\partial y} dx \quad (\text{A1})$$

along the center line $y = a/2$ (subscript c hereafter refers to this location). We evaluate (A1) using (22) and

$$\int_{|h'|>\lambda} \frac{1}{H} \left(\frac{H}{h'}\right)' dx = \int_{|h'|>\lambda} \left(\frac{1}{h'}\right)' dx + \delta \int_{|h'|>\lambda} \frac{1}{H} dx = \delta \int_{|h'|>\lambda} \frac{1}{H} dx. \quad (\text{A2})$$

The last equality follows because with the symmetry we assume

$$h'(H_{\max} + \lambda) = h'(H_{\min} - \lambda)$$

$$h'(H_{\max} - \lambda) = h'(H_{\min} + \lambda).$$

Using (22), (A1) can now be written as

$$\begin{aligned} \int_{h' > \lambda} \frac{\tau_c - \tau_a}{H} dx + \int_{h' < -\lambda} \frac{\tau_c - \tau_0}{H} dx - \int_{|h'| < \lambda} \frac{1}{H} \frac{\partial \psi}{\partial x} dx \\ = \int_0^1 \frac{\tau_c}{H} dx + \epsilon \int_0^1 \frac{1}{H^2} \frac{\partial \psi}{\partial y} dx. \end{aligned} \quad (\text{A3})$$

The last term on the left is the contribution of the internal boundary layers centered at H_{\max} and H_{\min} . Since H is constant to $O(\delta\lambda)$ within these layers

$$\int_{x_m-\lambda}^{x_m+\lambda} \frac{1}{H} \frac{\partial \psi}{\partial x} dx = \frac{\psi_{m+} - \psi_{m-}}{H_m} + \begin{cases} O(\delta\lambda^2 J_m), & \text{smooth topography} \\ O(\delta\lambda J_m), & \text{piecewise linear topography} \end{cases}$$

where subscript m is generic for min and max, J_m is the magnitude of the jump. The jumps may be evaluated using (22). If the topography is smooth, then

$$\begin{aligned} \psi(H_{\max+}) - \psi(H_{\max-}) &= T + \frac{H_{\max}}{\delta\lambda} (\tau_c - \tau_a) + \frac{H_{\max}}{\delta\lambda} (\tau_c - \tau_0), \\ \psi(H_{\min+}) - \psi(H_{\min-}) &= -\left(T + \frac{H_{\min}}{\delta\lambda} (\tau_c - \tau_a) + \frac{H_{\min}}{\delta\lambda} (\tau_c - \tau_0) \right). \end{aligned} \quad (\text{A4a})$$

For the piecewise linear topography (24)

$$\begin{aligned} \psi(H_{\max+}) - \psi(H_{\max-}) &= T + \frac{H_{\max}}{4\delta} (\tau_c - \tau_a) + \frac{H_{\max}}{4\delta} (\tau_c - \tau_0), \\ \psi(H_{\min+}) - \psi(H_{\min-}) &= -\left(T + \frac{H_{\min}}{4\delta} (\tau_c - \tau_a) + \frac{H_{\min}}{4\delta} (\tau_c - \tau_0) \right). \end{aligned} \quad (\text{A4b})$$

The net contribution to the left-hand side of (A3) from these jumps is, since $H_{\max} = 1 + \delta$ and $H_{\min} = 1 - \delta$,

$$\begin{aligned} \int_{|h'| < \lambda} \frac{1}{H} \frac{\partial \psi}{\partial x} dx &= \frac{\psi}{H_{\max}} \Big|_-^+ + \frac{\psi}{H_{\min}} \Big|_-^+ + O(\lambda) \\ &= \frac{2\delta}{1 - \delta^2} T + O(\lambda) = 2\delta T + O(\lambda). \end{aligned} \quad (\text{A5})$$

Substituting (22) and (A5) in (A3) yields

$$\begin{aligned} \tau_c \int_0^1 \frac{1}{H} dx - \tau_a \int_{h' > \lambda} \frac{1}{H} dx - \tau_0 \int_{h' < -\lambda} \frac{1}{H} dx + 2\delta T + O(\lambda) \\ = \tau_c \int_0^1 \frac{1}{H} dx - \frac{\epsilon}{\delta} \left(\frac{\partial \tau}{\partial y} \right)_c \int_0^1 \frac{1}{H h'} dx. \end{aligned} \quad (\text{A6})$$

The first terms on the right and on the left of (A6) cancel out; the last term on the right vanishes since H is assumed symmetric with respect to $h' = 0$. One finds

$$T = \frac{1}{2\delta} \left(\tau_a \int_{h' > \lambda} \frac{1}{H} dx + \tau_0 \int_{h' < -\lambda} \frac{1}{H} dx + O(\lambda) \right) = O(\delta^{-1}). \quad (\text{A7})$$

If, as assumed in (25) $\tau_0 = \tau_a = 0$, then the leading order dependence of T on the parameters would be *qualitatively* different. It follows from (21) that within the internal boundary layer the stream function satisfies

$$\epsilon \frac{\partial^2 \psi}{\partial x^2} + \delta h' \frac{\partial \psi}{\partial y} = 0,$$

so the width of this boundary layer is

$$\lambda = \begin{cases} O((\epsilon/\delta)^{1/3}), & \text{smooth topography} \\ O((\epsilon/\delta)^{1/2}), & \text{piecewise linear topography.} \end{cases} \quad (\text{A8})$$

Finding an asymptotic approximation of the f -plane transport requires resolving the complicated structure of the internal boundary layers similarly to Kamenkovich and Mitrofanov (1971). However, some conclusions can be drawn from (A7), (A8). Since $\lambda \rightarrow 0$ as $\epsilon \rightarrow 0$, it follows that $T \rightarrow 0$ as $\epsilon \rightarrow 0$. Keep in mind, this assumes $\epsilon > 0$ and no additional physics such as nonlinearities. Faster growth of the internal boundary layer thickness with ϵ/δ in the case of piecewise linear topography implies sharper dependence of the transport on ϵ, δ in this case (cf. Fig. 3a, b).

If $\tau_0 = \tau_a \neq 0$ the numerical solution exhibits behavior predicted by (A7). The transport is independent of friction to leading order and varies inversely with δ (Fig. 3a, b). If $\tau_0 = \tau_a = 0$ (A7) and (A8) predict

$$T = \delta^{-1}(\epsilon/\delta)^\alpha, \quad (\text{A9})$$

where

$$\alpha = \begin{cases} \frac{1}{3}, & \text{smooth topography} \\ \frac{1}{2}, & \text{piecewise linear topography.} \end{cases}$$

Numerical experiments agree with the form (A9), but with $\alpha \approx 0.5$ in the case of

smooth topography and $\alpha \approx 0.65$ in the case of piecewise linear topography (Fig. 3a, b). In both cases the experimental α is approximately $\frac{1}{6}$ greater than the analytic estimate.

The zero order total energy input on the f-plane may be evaluated using (22):

$$-\int_{|h'|>\lambda} dx \int_0^a \frac{\tau}{H} \frac{\partial \psi}{\partial y} dy = \frac{\tau_a^2 - \tau_0^2}{2\delta} \left(\int_{h'>\lambda} \frac{1}{h'} dx + \int_{h'<-\lambda} \frac{1}{h'} dx \right) = 0$$

with the assumed symmetry in H .

REFERENCES

- Bryan, K. and M. D. Cox. 1972. The circulation of the World Ocean: A numerical study. Part I, a homogeneous model. *J. Phys. Oceanogr.*, 2, 319–335.
- Bye, J. A. T. and T. W. Sag. 1972. A numerical model for circulation in a homogeneous world ocean. *J. Phys. Oceanogr.*, 2, 305–318.
- Hidaka, K. and M. Tsuchiya. 1953. On the Antarctic Circumpolar Current. *J. Mar. Res.*, 12, 214–222.
- Holloway, G. 1987. Systematic forcing of large-scale geophysical flows by eddy-topography interaction. *J. Fluid Mech.*, 184, 463–476.
- Ichiye, T. 1976. Contributions to the dynamics of the Antarctic Circumpolar Current (A.C.C.) (Integral relationship). Department of Oceanography, Texas A&M Univ., 24 pp.
- Ivanov, Yu. A. and V. M. Kamenkovich. 1959. Bottom relief as a basic factor contributing to the lack of zoning in the Antarctic Circumpolar Current. *Doklady Akademii Nauk SSSR*, 128, 977–979 (Translated from Russian).
- Johnson, J. A. and R. B. Hill. 1975. A three-dimensional model of the Southern Ocean with bottom topography. *Deep-Sea Res.*, 22, 745–751.
- Kamenkovich, V. M. 1960. The influence of bottom relief on the Antarctic Circumpolar Current. *Doklady Akademii Nauk SSSR*, 134, 983–984 (Translated from Russian).
- 1961. The integration of the marine current theory equations in multiply connected regions. *Doklady Akademii Nauk SSSR*, 138, 629–631 (Translated from Russian).
- 1962. On the theory of the Antarctic Circumpolar Current. *Trudy Instituta Okeanologii*, 56, 245–306 (Translated from Russian).
- Kamenkovich, V. M. and V. A. Mitrofanov. 1971. An example of the effect of ocean-bottom topography on currents. *Doklady Akademii Nauk SSSR*, 199, 8–10 (Translated from Russian).
- McWilliams, J. C., W. R. Holland and J. H. S. Chow. 1978. A description of numerical Antarctic Circumpolar Currents. *Dyn. Atmos. Oceans*, 2, 213–291.
- Munk, W. H. and E. Palmen. 1951. Note on the dynamics of the Antarctic Circumpolar Current. *Tellus*, 3, 53–55.
- Naik, N., M. Cane, M. Israeli and S. Basin 1994. A solver for the barotropic mode in the presence of variable topography and islands. *Mon. Wea. Rev.*, (submitted).
- Stommel, H. 1948. The westward intensification of wind-driven ocean currents. *Trans. Am. Geophys. Union*, 99, 202–206.
- 1957. A survey of ocean current theory. *Deep-Sea Res.*, 4, 149–184.
- Treguier, A. M. and J. C. McWilliams. 1990. Topographic influences on wind-driven, stratified flow in a β -plane channel: an idealized model for the Antarctic Circumpolar Current. *J. Phys. Oceanogr.*, 20, 321–343.

- Wang, L. and R. X. Huang. 1994. Topographic control of the Antarctic Circumpolar Current. Part 1: A linear homogeneous channel model. (in preparation).
- Whitworth, T. III. 1983. Monitoring the transport of the Antarctic Circumpolar Current in Drake Passage. *J. Phys. Oceanogr.*, *13*, 2045–2057.
- Wolff, J.-O., V. O. Ivchenko, A. V. Klepikov and D. J. Olbers. 1990. On the effects of topography on the dynamics of zonal currents in the ocean. *Doklady Akademii Nauk SSSR*, *313*, 323–327 (Translated from Russian).
- Wolff, J.-O., E. Maier-Reimer and D. J. Olbers. 1991. Wind-driven flow over topography in a zonal β -plane channel: a quasi-geostrophic model of the Antarctic Circumpolar Current. *J. Phys. Oceanogr.*, *21*, 236–264.
- Wolff, J.-O., and D. J. Olbers. 1989. The dynamical balance of the Antarctic Circumpolar Current studied with an eddy resolving quasi-geostrophic model, in *Mesoscale-Synoptic Coherent Structures in Geophysical Turbulence*, J. C. J. Nihoul and B. M Jamart, eds., Elsevier, 435–458.

Received: 25 August, 1992; revised: 5 October, 1993.